Experimental investigation of the melting transition of the plasma crystal

A. Melzer, A. Homann, and A. Piel
Institut für Experimentalphysik, Christian-Albrechts-Universität Kiel, Olshausenstraße 40-60, D-24098 Kiel, Germany
(Received 31 July 1995)

Measurements of the melting transition of a Coulomb crystal consisting of dust particles immersed in a rf parallel plate discharge in helium were performed. The dust crystal is shown to be solid at higher gas pressure (120 Pa) and low discharge power (10–20 W). Reducing the gas pressure or increasing the discharge power leads to fluid states of the dust ensemble. Even gaslike states are observed at low pressures of about 40 Pa. The transition is attributed to an increasing effective particle temperature. The phase transition is compared with one-component-plasma and Yukawa models and with basic predictions of theories for two-dimensional melting.

PACS number(s): 52.25.Vy, 64.70.−p

I. INTRODUCTION

The physics of dusty plasmas has attracted a growing interest in the fields of technological applications, in astrophysics, and very recently in the field of condensed matter. Dust, i.e., particles of nanometer to micrometer size, is produced in rf plasma etching devices as a product of sputter processes or by polymerization and agglomeration of reactive gas species. These particles are easily trapped by the strong electric fields in the sheath. Such particles can seriously affect the quality of the etching product [1]. In astrophysical situations dust in plasma is found in planetary rings, in interplanetary and interstellar clouds, as well as in comets [2].

Particles immersed in a laboratory plasma usually acquire a negative charge because of the higher diffusive flux of electrons compared to ions. These charged particles interact by means of their Coulomb repulsion and therefore form a strongly coupled system. In the late 1930s, Wigner [3] gave conditions under which a system consisting of ions in an electron background should "crystallize," in the sense of forming regular lattices, the so-called Wigner or Coulomb crystal. Ikezi [4] adopted these ideas for the case of dust particles in a plasma and derived the necessary plasma conditions under which the dust particles should form regular patterns (plasma crystal).

Very recently Chu and co-workers [5–7], in a magnetron discharge, studied particles produced in a silane-oxygen-argon gas mixture that are trapped in a groove around the rf electrode. The dust particles were found to form regular three-dimensional lattice structures. Moreover, raising the rf power leads to disorder in the arrangement of the dust particles. Thomas *et al.* [8] studied dust crystal formation in a parallel plate rf discharge in argon with monodisperse spherical plastic particles of 7 μm diameter added. The particles were found to be trapped in the sheath of the lower electrode. The grains arranged themselves in a flat crystal of many layers with hexagonal order. Melzer *et al.* [9,10] used a similar discharge geometry to perform *in situ* charge measurements of particles that form Coulomb lattices.

Colloidal suspensions, i.e., charged particles immersed in an aeqeous solution, provide a similar physical system in which Wigner crystallization and melting of two-dimensional crystals were studied [11]. The dynamics of the melting transition in two dimensions is of great interest since there exist contradictory theoretical and experimental results for the behavior of two-dimensional melting [12].

The plasma crystal is ideally suited for the investigation of two-dimensional melting, because the individual particles are easily observable and the dust-plasma system reacts to variations of discharge conditions within a few seconds in contrast to relaxation times of many hours for colloidal suspensions. We present here measurements of the phase transition of a two-dimensional plasma crystal. Monodisperse melamin-formaldehyde spheres of 9.4 μm diameter are used in a parallel plate rf helium discharge. The phase transition can be induced in two ways, either by raising the rf power or by reducing the pressure. The transition is monitored by a video camera and quantitatively analyzed by means of positional and orientational correlation functions. The particle dynamics during the melting process is indicated by the particles' trajectory plots.

II. CHARGE MEASUREMENT

A particle immersed in a plasma is hit by ions and electrons and in the absence of photoemission and secondary emission acquires a negative potential ϕ that repels the electrons and attracts the ions in such a way that the net average current to the particle is zero. The particle attains the floating potential like an isolated Langmuir probe. Since the particle can be viewed as a small spherical capacitor its charge therefore is $Q = 4\pi\epsilon_0 a\phi_{\mathrm{fl}}$, where ϵ_0 is the permittivity of free space, a is the particle's radius, and ϕ_{fl} is the floating potential.

The theoretical determination of the dust charge in the sheath region is very complicated since electron and ion distribution functions in the sheath have to be known. It is therefore necessary to measure the charge directly in

the plasma. We present here only a short description of the charge measurement method; details were published elsewhere [9,10]. The dust particles in rf discharges are suspended in the sheath of the lower electrode where the upward electric field force $F_E = QE$ balances the weight $F_g = m_d g$ of the particle. In the vicinity of the particle's equilibrium position the electric and gravitational force form a parabolic potential well. It is possible to excite resonant oscillations of the particle in this potential well, e.g., by modulating the rf voltage with a small low-frequency voltage. The particles charge is determined from the resonance frequency ω_0

$$\omega_0^2 = \frac{Qn_i e}{\epsilon_0 m_d} , \tag{1}$$

where $m_d = 6.73 \times 10^{-13}$ kg is the mass of the particle and n_i is the ion density, which is related to the electric field via the Poisson equation. The ion density is measured in the bulk of the discharge with Langmuir probes and the obtained value is extrapolated into the sheath region.

III. STRONGLY COUPLED SYSTEMS

The dust particles are strongly coupled by their Coulomb repulsion. A crucial parameter for the description of these strongly coupled systems is the coupling parameter Γ, which gives the electrostatic energy of nearest neighbors in units of their thermal energy

$$\Gamma = \frac{Q^2}{4\pi\epsilon_0 bkT_d} . \tag{2}$$

Here k is the Boltzmann constant, T_d is the dust temperature, and b is a scale length of the order of the nearest-neighbor distance b_{NN}. In three dimensions $b = (\frac{4}{3}\pi n_d)^{-1/3}$, whereas in two dimensions $b = (\pi n_d)^{-1/2}$; n_d is the three- and two-dimensional dust density, respectively.

The one-component plasma (OCP) describes the fundamental strongly coupled system of one charged species immersed in a homogeneous background of opposite charges [13]. The particles interact with a Coulomb potential $\psi_C(r) = Q/(4\pi\epsilon_0 r)$. The three-dimensional system is found to form regular, crystalline patterns for values of Γ greater than $\Gamma_c = 170$. For the two-dimensional system $\Gamma_c = 130$. For smaller Γ values the system is in a fluid state [14]. For very small values of Γ ($\Gamma < 5$) the state is gaslike.

In more refined models shielding effects by the background charge are taken into account, which changes the interaction potential to the Debye-Hückel or Yukawa type: $\psi_{\mathrm{DH}}(r) = Q/(4\pi\epsilon_0 r)\exp(-r/\lambda_D)$. Then Γ_c becomes a function of the screening strength $\lambda = b/\lambda_D$, where λ_D is the Debye length. Robbins *et al.* [15] performed simulations on these Yukawa systems and found that Γ_c rises approximately exponentially with λ. The OCP model is the limit of $\lambda = 0$ of this Yukawa model.

IV. EXPERIMENTAL SETUP

The rf parallel plate discharge consists of a lower, powered aluminum electrode of 15 cm diameter and an upper grounded grid mesh electrode of approximately 1 cm in mesh size (see Fig. 1). The discharge gap is 6 cm wide. The electrodes are placed in a vacuum tank of 50 cm diameter and 70 cm height with four horizontal and one top viewport. The rf generator $f = 13.56$ MHz with maximum rf power output of 300 W is connected to the lower electrode through a matchbox and a blocking capacitor. The discharge is operated in helium.

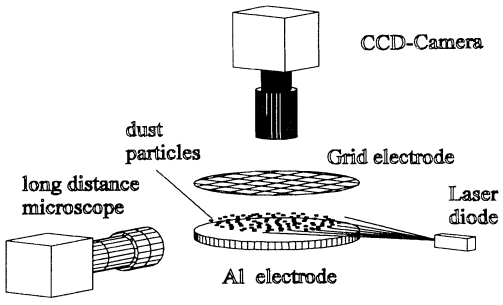

FIG. 1. Experimental setup dust particles in the sheath of the lower electrode are illuminated by a horizontally expanded laser beam from the laser diode. The individual dust particle layers are viewed in scattered laser light from the top. From the side the resonance of the particles is observed from another video camera. Therefore a vertically expanded laser beam is used (not shown).

We use monodisperse melamin-formaldehyde spheres of 9.4 ± 0.3 μm diameter [16]. This dust is contained in a dust dropper within the vacuum vessel above the upper electrode. The particles suspended in the lower sheath are illuminated by a horizontally expanded thin sheet of laser light from a laser diode that is sufficiently constricted vertically to study individual layers of the crystal. The dust particle layers are viewed in scattered light with a video camera from top through the grid electrode. A second HeNe-laser beam is vertically expanded to illuminate a cross section of the crystal in order to measure the resonance of the particles and to investigate the layer structure of the crystal. Through a side window the particles are observed by a second video camera. The video signals are stored by a video-tape recorder or are transferred to computer via a frame-grabber card.

V. RESULTS AND DISCUSSION

The melting transition from ordered structures to fluid and even gaslike states of the dust particles in the sheath of the lower electrode can be induced either by raising the discharge power or by decreasing the gas pressure. Plasma crystals with two or more layers are found to undergo these transitions. The higher the number of layers the more disordered the whole crystal. Moreover, the layers nearest the electrode melt first (i.e., at higher pressure or lower power) and show more violent particle motion, while the uppermost layer stays solid longest. To have relatively simple conditions we present the melting tran-

sition for a crystal consisting of two layers only. In all of the plots below the upper layer is shown.

A. Melting by reducing the gas pressure

Gas pressure was reduced from 118 to 39 Pa, while the discharge power was fixed at 12 W. A certain amount of dust particles was inserted at the beginning of the experiment and it was not changed during the transition. At 118 Pa [see Fig. 2(a)] the dust particles form a regular hexagonal lattice. A Wigner-Seitz (WS) cell analysis yields that 91.5% of the WS cells are hexagons with almost all having the same size. One also finds 4.4% of five-sided and 4.1% of seven-sided cells. The pair correlation function $g(r)$ (Fig. 3), which gives the probability of finding two dust particles separated by a distance r, reveals that the positional order is maintained for at least five nearest-neighbor distances. The nearest-neighbor distance b_{NN} is 450 μm. The vertical lines at the bottom of Fig. 3 show the positions of particles in an exact hexagonal lattice. The crystal consists of two hexagonal layers, as can be seen from Fig. 2(b), the particles of the lower layer being located exactly below a particle of the upper layer. This vertically aligned arrangement is apparently not a minimum energy configuration if one considers only the Coulomb or Yukawa interaction of the particles.

Figure 4 shows the pair correlation functions at various pressures. At high pressure the correlation function shows ordered structures over large distances at least up to 3000 μm. At approximately 76 Pa, the length up to

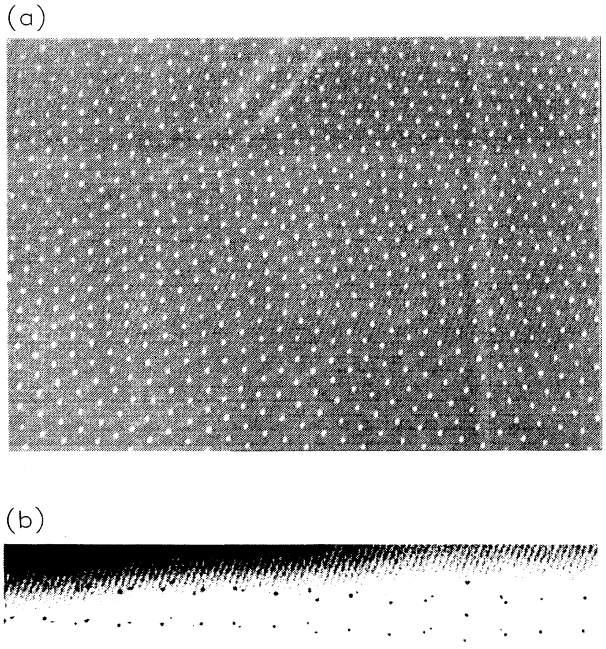

FIG. 2. Video images of the Wigner crystal at 118 Pa seen (a) from the top and (b) from the side (inverted image).

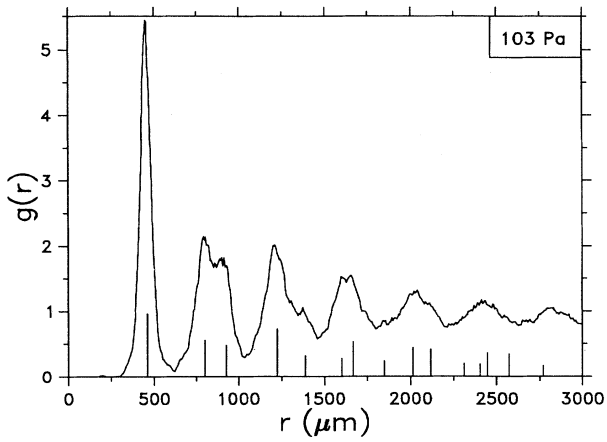

FIG. 3. Pair correlation function at 103 Pa. The vertical lines mark the positions for an ideal hexagonal lattice. The correlation length is at least five nearest-neighbor distances.

which ordering is observable begins to decrease rapidly and, at 39 Pa, the correlation function shows no order at all. It resembles that of an ideal gas. So these correlation functions indicate that a transition from an ordered solid structure to a fluid and finally to a gaslike situation has taken place. It is noteworthy that the nearest-neighbor distance $b_{NN} = 450$ μm is nearly unchanged during the pressure reduction.

To investigate the dynamics of the particles during the melting transition the trajectories of individual particles have been recorded. For this purpose, a series of 11 snapshots of the dust particles are taken at 1-s intervals. The individual particles' positions are traced with a line through the series of snapshot images. When a particle does not move during this time it appears as a small dot; otherwise it forms a more or less extended trajectory. This analysis was applied for various pressure settings

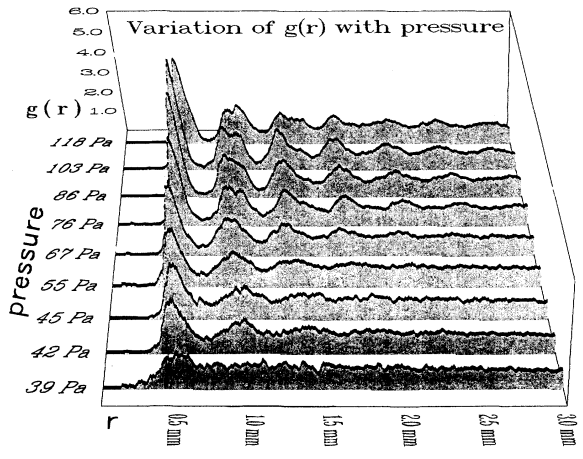

FIG. 4. Variation of the pair correlation function with pressure. At high pressure well ordered particles are observed. When decreasing the pressure the correlation becomes less. At 39 Pa the correlation function is almost that of an ideal gas.

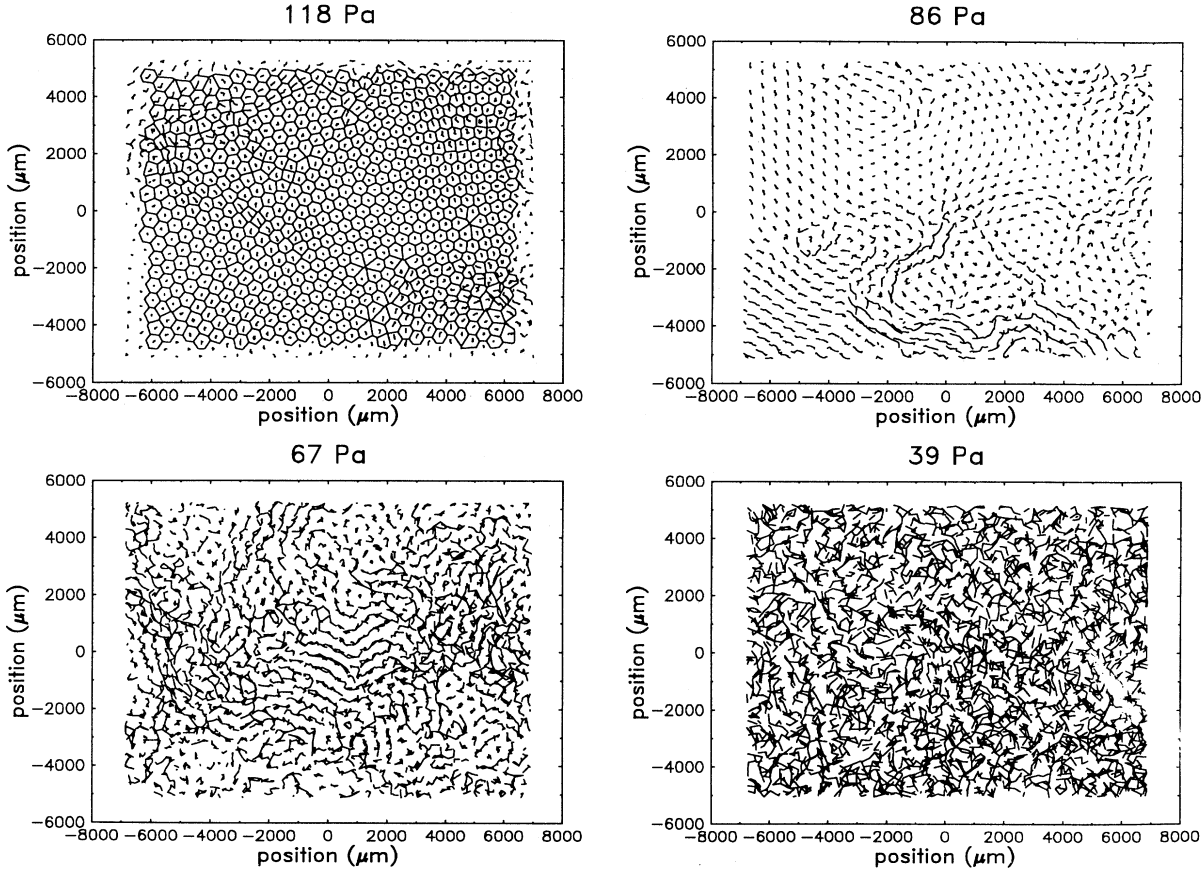

FIG. 5. Particles' trajectories over 10 s. (a) 118 Pa, (b) 86 Pa, (c) 67 Pa, and (d) 39 Pa.

in the mentioned range. Figure 5(a) shows such a plot for a pressure of 118 Pa. For illustration, the WS cell construction for the first snapshot is also included in this figure. Mainly the particles do not move but stay in their individual WS cells. Only at the edges there is some particle motion observable. At a pressure of 86 Pa [Fig. 5(b)] there are some regions where the particles stay in their initial position and in other regions the particles move along streamlines at the boundary of the crystalline regions. Note that the trajectories do not intersect, which is typical of fluid motion. The motion is further enhanced at 67 Pa [Fig. 5(c)]. Here streamlines are clearly observable, but there are some regions in which the particle motion becomes not aligned in streamlines. Finally, in Fig. 5(d) at 39 Pa there is no ordered motion observable. The particle motion becomes irregular. Because of the time steps of 1 s, it is not evident in these snapshots that at reduced gas pressure some particles begin to oscillate about their equilibrium position at a frequency of approximately 10 Hz. The number of oscillating particles and the oscillation amplitude increases during pressure reduction.

From the above results we refer to the dust particle arrangement as the solid or crystal state at pressures of above 100 Pa, as the fluid state below that value, and as a gaslike state at the lowest pressure values.

B. Comparison with OCP and Yukawa models

Now the measured values of Γ can be compared with the theoretical predictions of the OCP model and the Yukawa model of Robbins *et al.* [14,15]. Γ is calculated from the measured dust particle charge Q according to Eq. (1) (see Fig. 6), the measured scale length b, and the dust temperature T_d. In view of the friction with the gas

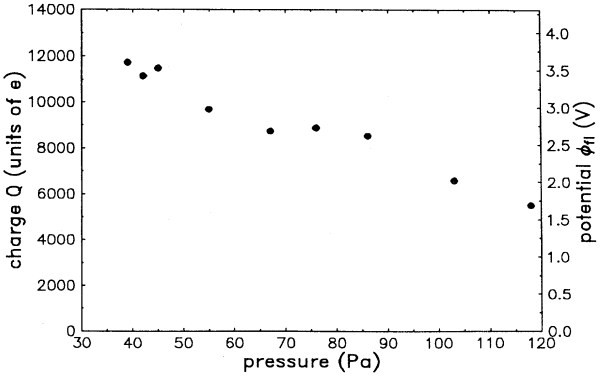

FIG. 6. Measured charge and the corresponding potential of the dust particles as a function of gas pressure.

background it may be anticipated that the dust particles attain a kinetic energy close to room temperature. In their experiment with argon at 200 Pa Thomas *et al.* [8] determined the particle temperature to be 310 K and this temperature was used in the calculation of Γ in recent works [8–10]. This assumption, however, needs a critical review at low pressure values. At room temperature the thermal velocity $v_{\rm th} = \sqrt{2kT_d/m_d}$ of the dust particle is about 100 μm/s. The dust particle motion, however, appears to be irregular with a much higher speed at lower pressures. Therefore the actual dust particle temperature has to be measured.

For the experimental determination of the dust thermal energy again video sequences of the particles were taken, but now at the video frame rate of 50 frames per second. From the motion of the particles during this small interval of 20 ms an effective dust temperature is deduced. The results are shown in Fig. 7. Figure 7(a) shows the velocity distribution in two orthogonal directions (top and middle plot) for 39 Pa. The distribution of $v = (v_x^2 + v_y^2)^{1/2}$ is shown in the bottom plot. The dust temperature was deduced from their mean kinetic energy $E = \frac{1}{2}m\langle v_{x,y}^2\rangle = \frac{1}{2}kT_{x,y}$ and $E = \frac{1}{2}m\langle v^2\rangle = 2\frac{1}{2}kT$, respectively. The distribution functions are found to be Maxwellian and therefore one can speak of an effective kinetic dust temperature T_d. Figure 7(b) shows the measured "thermal" energy of the dust particles with pressure. The absolute values of these temperatures are unexpectedly high. At the highest observed random kinetic energy of approximately 50 eV the particles move about 90 μm per frame. Since the particles carry more than 5000 elementary charges a dc potential difference of only 10 mV is sufficient to give the particles such a high energy. Finally, one can see in Fig. 7(b) that at higher pressure the temperature saturates at 0.7 eV. This value is an instrumental limit given by the pixel structure of the video camera. Presently 0.7 eV is the smallest temperature to be measured by our camera arrangement.

Figure 8 shows the measured values of Γ as a function of the screening strength λ. The screening strength is determined from the ion density; an electron contribution to screening is neglected because of the reduced average electron density in the sheath. The theoretical melting lines of the OCP and Yukawa model are indicated. The circle symbols show the values of Γ calculated from the measured dust temperature, the numbers indicating the respective values of the gas pressure. Γ values derived from a dust temperature of $T_d = 300$ K are also included for comparison (squares). It can be seen that the solid states are found with corresponding values of Γ in the range 1000–2000. These values of the coupling parameter are approximately ten times larger than the critical values for the two-dimensional OCP model. The Yukawa model predicts higher values of Γ for our observed screening strengths or lower values of λ for the measured Γ. With reduced gas pressure Γ drops dramatically due to the higher dust temperature. At the lowest pressure of 39 Pa, where the gaslike situation is found, Γ =3. From comparing the pair correlation function for 39 Pa with those obtained from simulations (e.g., [13]) one would have expected Γ to be of the order of 10. In contrast, the assumption of a constant dust temperature of 300 K leads to rising values of Γ when the system moves to the fluid and gaslike state. Finally, it can be seen that the enormous increase of the dust particle temperature forces the system from the solid to a fluid and gaslike state.

The processes leading to the observed high particle temperatures are not known. As a precursor for the erratic motion we observed oscillations of the particles about their equilibrium positions during the melting process, where the oscillation amplitude of the particle in the lower layer is greater than that of the corresponding one in the upper layer and a phase difference of 45–90° is observable. The oscillatory and erratic kinetic energy of the dust particles is dissipated through friction with the neutral gas background. In order to balance this energy loss we assume that the particles gain energy from the directed ion flux that flows from the bulk plasma onto the electrode. Additionally, some shadowing effects of the ion motion by the particles of the upper layer may play a role in the formation of the vertical alignement as a stable particle configuration.

C. Comparison with theories of two-dimensional melting

There exist two competing approaches to the phase transition in two dimensions: first the Kosterlitz-Thouless-Halperin-Nelson-Young (KTHNY) theory of melting [17–19,12], which predicts two continuous transitions from the solid to the fluid state via an intermediate state, the so-called hexatic phase, and second, a theory [20,12] that predicts a single first-order transition. We present here only a short description of the main findings of these theories. For further discussion see Ref. [12].

The KTHNY theory assumes definite formations of defects during the melting process. In our situation defects are dust particles that do not have six but five or seven nearest neighbors, so-called disclinations. A dislocation, i.e., a row of dust particles that sticks partly into the crystal, can be viewed as a 5-7 pair of disclinations. In the solid state only pairs of dislocations (quartets of 5-7-5-7 disclinations) occur. Moreover, positional and orientational order of the dust particles is found. The fluid state is reached by two continuous transitions. In the first step pairs of dislocations unbind into free dislocations (pairs of 5-7 disclinations). The resulting phase is called a hexatic phase, because in this phase the positional order is destroyed, but still orientational order is found. The next transition leads to an unbinding of the disclination pairs into free disclinations leading to a destruction of the orientational order. This state is now the fluid state.

The theory predicting a first-order transition starts with the existence of grain boundaries. These grain boundaries induce a first-order transition to the fluid state without an intermediate phase. Grain boundaries can be viewed as rows of 5-7-5-7 . . . disclinations.

For the analysis of the orientational order the bond-angular correlation function $g_6 = \langle \exp[6i(\theta(0) - \theta(r))]\rangle$ is used. Here $\theta(r)$ is the angle of a bond at position

r between a particle and its nearest neighbour relative to a fixed axis [12]. In the solid state the correlation function g_6 should be constant, in the hexatic phase (only for the KTHNY theory) g_6 approaches a power law with a fixed range of exponents [$g_6(r) \propto r^{-\eta}$, $\eta > 0.25$], and in the fluid state the correlation function should decay exponentially.

By this means we have analyzed the orientational correlation during the melting process. g_6 is shown in Fig. 9 for various pressures. One can see that at pressures of

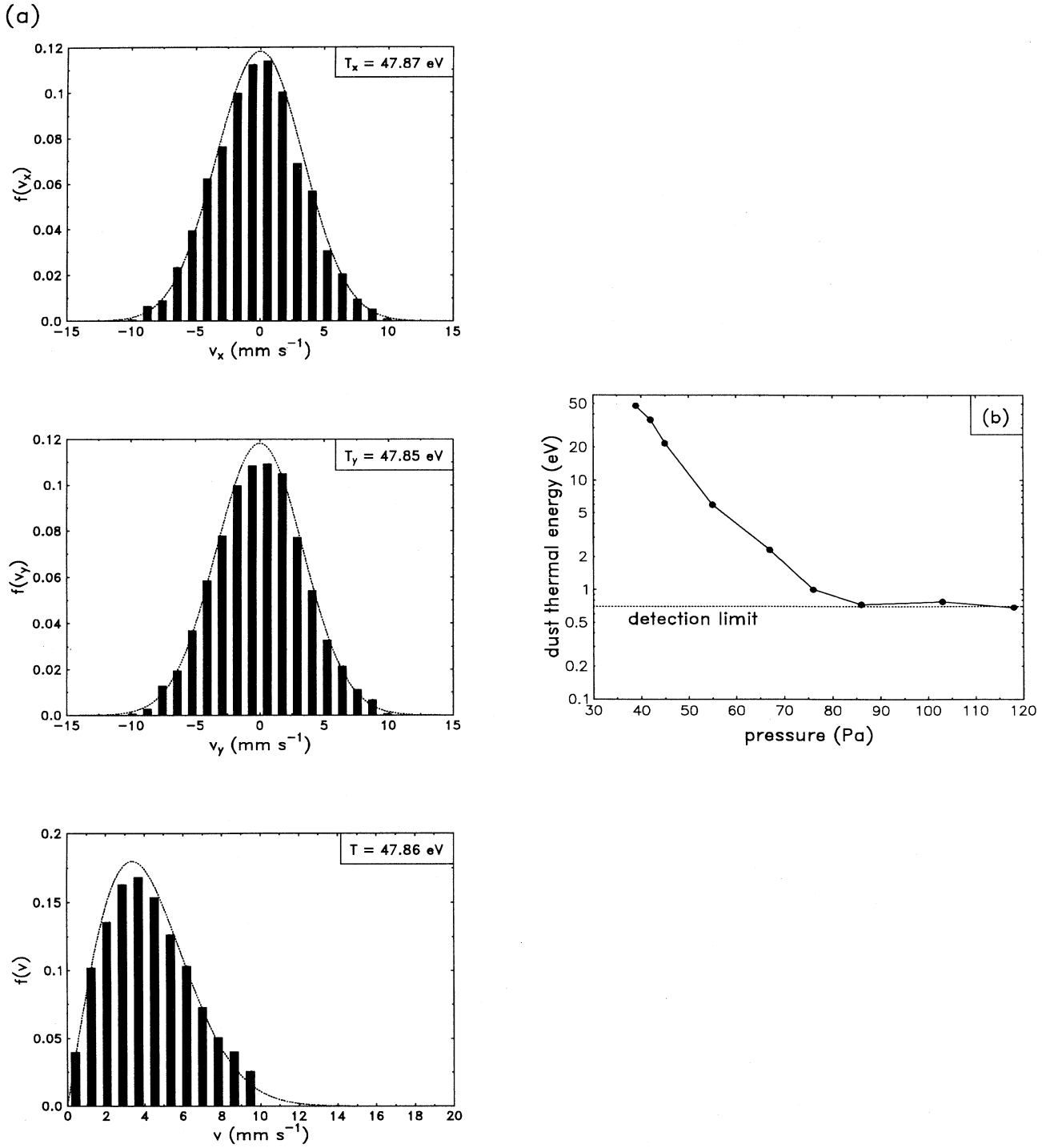

FIG. 7. (a) Velocity distribution of dust particles at a pressure of 39 Pa. Top and middle, distribution in two perpendicular directions; bottom, distribution of $v = (v_x^2 + v_y^2)^{1/2}$. Maxwellian velocity distribution functions calculated from the measured temperature are also indicated (dashed line) for comparison. (b) Thermal energy of the dust particles as a function of pressure.

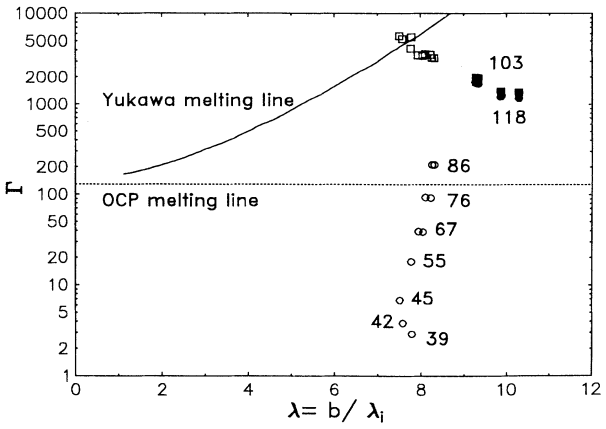

FIG. 8. Comparison of measured coupling parameters Γ with theoretical predictions of OCP and Yukawa coupled systems for the melting by pressure reduction. Solid line, Yukawa melting line; dashed line, OCP melting line; ○, values of Γ with measured temperature; □, values of Γ with dust temperature at room temperature. Full symbols denote solid states. The numbers give the corresponding pressure values.

118 and 103 Pa the correlation function is constant or very slowly decaying up to $r = 5000$ μm, which is more than ten times the interparticle distance. This indicates that there is a long-range orientational order present in the crystal. When the pressure is reduced g_6 is decaying more and more rapidly. At 39 Pa no angular correlation is observable at all. We tried to fit our measured g_6 functions with power laws or exponentials. The exponents found for a power-law decay of $g_6(r)$ are about 0.36. The same functions can be fitted with an exponential decay with $0.002/\mu$m at 67 Pa and $0.000\,35/\mu$m at 103 Pa. These fit functions show convincing agreement

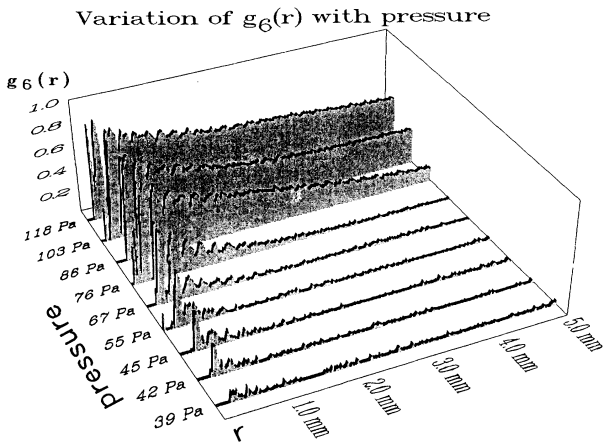

FIG. 9. Variation of the angular correlation function $g_6(r)$ with pressure. At higher pressure the correlation function is nearly constant and is rapidly decaying at lower pressure.

only for a limited range of r up to 5-10 nearest-neighbor distances, but for a larger range of r both laws fit quite poorly.

Figure 10 shows the defect plots at various pressures. At 118 Pa one can see dislocation pairs as well as free dislocations, but also some chainlike arrangements of de-

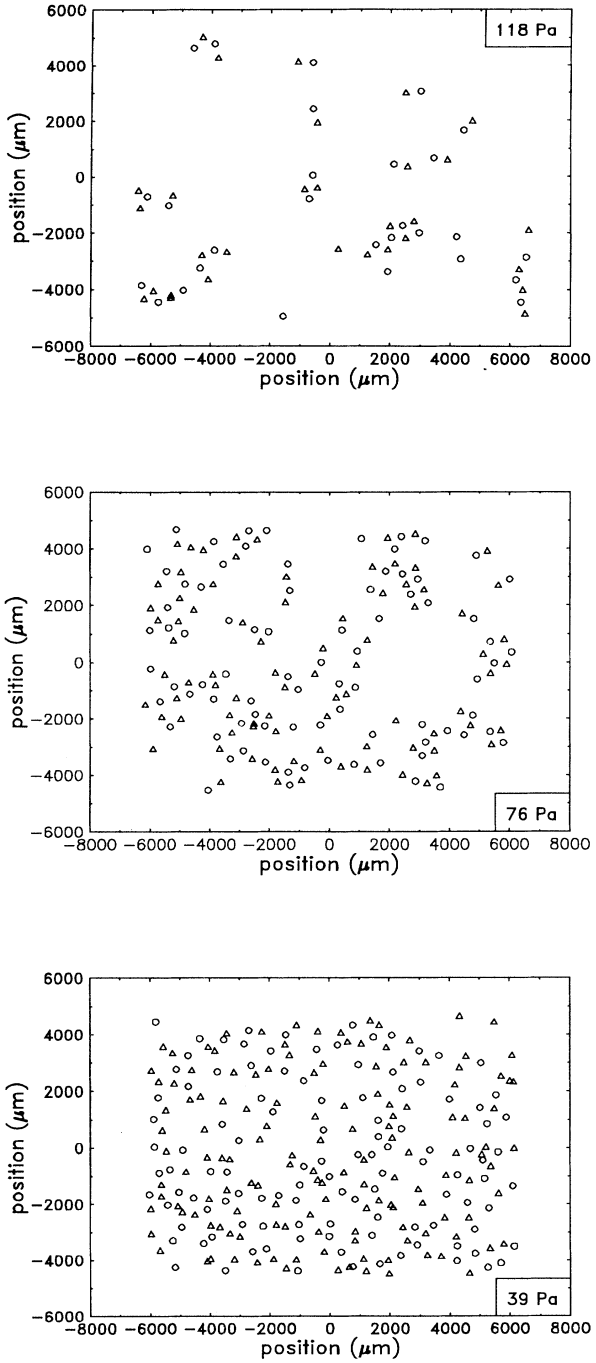

FIG. 10. Defect plot for 118, 76, and 39 Pa. Triangles denote five-coordinate and circles seven-coordinate particles. Grain sites with six nearest neighbors are not shown for clarity.

fects. When the pressure is reduced the number of defects is increasing and the defects arrange more and more in chains. These chains separate crystalline regions that are slightly rotated with respect to each other. This rotation leads to a decay in the angular correlation function g_6, which is not dealt with in the KTHNY theory of melting. The rotated crystal regions indicate some similarity to the grain-boundary-induced theory of melting. But the observed transition seems not to be first order since the angular and positional correlations change continuously within a pressure range. In this way our melting transition shows features of both theories for the two-dimensional melting, though one has to bear in mind that our crystal is not strictly two dimensional but consists of two layers.

Dubin [21] has addressed the problem of the crystal structure of a horizontally infinite crystal in a vertical harmonic potential well. This is a situation that is similar to our conditions where we have a laterally extended crystal that is vertically confined by gravity and electric forces. They found in their simulations that the crystal structure depends on the density of the dust particles. They observed hexagonal order for one-layer crystals, but crystals with two or more layers can have hexagonal, bcc, or fcc structure. In our experiment we only found hexagonal order. From the experiments we saw that a particle of the lower layer always is located directly below one of the upper layer, so the upper layer defines the positions for the lower layer. Thus the structure of the two-layered crystal is determined only by the upper layer, which is always hexagonal.

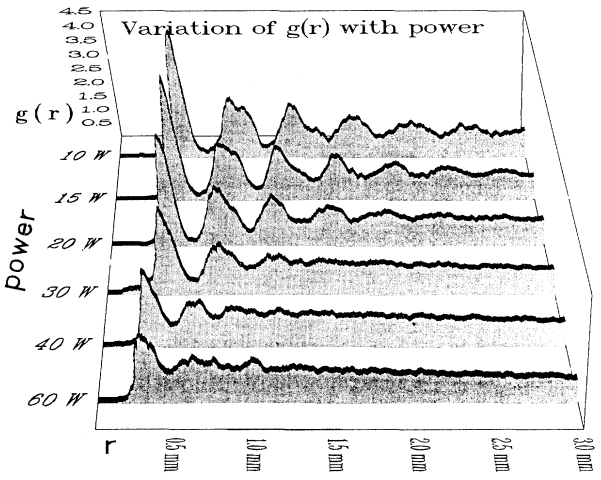

FIG. 11. Variation of the pair correlation function with power. The positional order decreases with power, but a gaslike state is not reached. Note that the nearest-neighbor distance is decreasing with power.

VI. MELTING BY INCREASING THE DISCHARGE POWER

Besides the melting transition by reducing the gas pressure increasing the discharge power leads to melting of the dust crystal too. Figure 11 shows the pair correlation functions with increasing power at a fixed pressure of 100 Pa. The positional order of the dust particle is decreasing with increasing power. At a power of 10 W (V_{PP} = 80 V) the particles' positions are ordered at least up to six nearest-neighbor distances, whereas at 60 W (V_{PP} = 180 V) only the nearest-neighbor and next-nearest-neighbor ordering is observable. Here two differences from the melting by pressure reduction can be noticed. The first one is that the interparticle distance is decreasing from 480 μm at 10 W to 340 μm at 60 W. The other difference is that a gaslike state is not reached in this and in a further extended power range.

In Fig. 12 the particle trajectories are shown. At 10 W the particles do not move; the crystal is solid. At 30 W (V_{PP} = 125 V) the particle motion is very slow. For 10 s the particle trajectories are not overlapping yet. At 40 W (V_{PP} = 150 V) streamlines surrounding regions of small motion are observable. Here one can speak of a fluid motion. The streamlines are dominating at 60 W and there seems to be only small erratic motion, although the dust particles show an oscillatory motion about their equilibrium positions with a frequency in the range 10–20 Hz. But this oscillation does not lead to such an erratic motion as observed at low pressure, because of the high damping. At 40 and 60 W it is obvious that the interparticle distance is not constant in these plots. When increasing the discharge power the particles move closer together, which hints at a decreasing Debye length due to increased ion density with power. Then the outer parts of the dust cloud come into the field of view of the video camera. In these outer parts the interparticle distance is larger than that in the center of the crystal. The broadening of the peaks due to this difference in the separation of the dust particles superposes the destruction of the positional order in these fluid states.

A comparison of the measured values of Γ with the OCP and Yukawa model is done in Fig. 13. The symbols show the values of Γ with the measured temperature. The measured dust temperature is only slightly above the detection limit for power values of 40 W and more. Below this power the temperature is at this limit and then the dust temperature is assumed to be room temperature, which certainly leads to an overestimation of Γ for power values somewhat below 40 W. But again the solid states are found at values of Γ of the order 500 up to 1000, which again is a range between the predictions of the OCP and the Yukawa model. By the melting due to pressure reduction the screening strength decreased slightly due to the decreasing ion density and unchanged inter-particle distance. At the transition by raising the power both the ion density and the interparticle distance are changing, leading to an almost constant screening strength. So here the particle oscillations and the so-

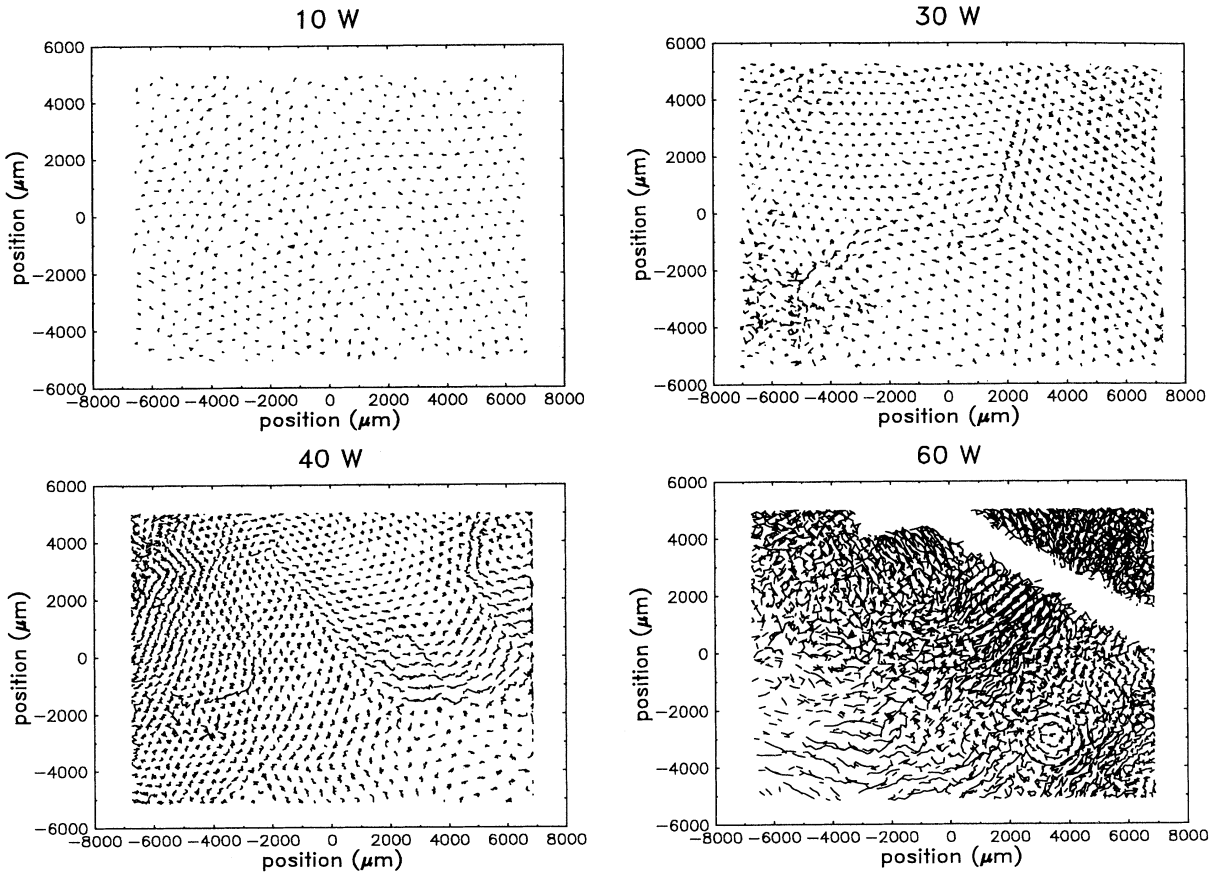

FIG. 12. Particles' trajectories over 10 s. (a) 10 W, (b) 30 W, (c) 40 W, and (d) 60 W. The white bar at 60 W is a part of the grid mesh electrode located in the field of view of the video camera.

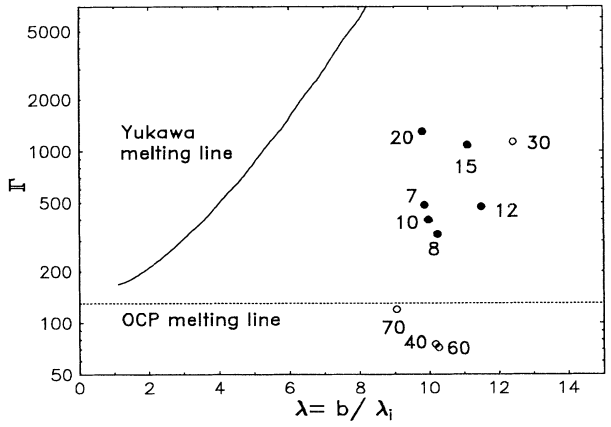

FIG. 13. Comparison of measured coupling parameters Γ with theoretical predictions of OCP and Yukawa coupled systems for the melting by raising the power. Solid line, Yukawa melting line; dashed line, OCP melting line; ○, values of Γ with the measured dust temperature. Full symbols denote solid states. The numbers give the corresponding power values.

enhanced particle temperature leads to the melting of the crystal too.

VII. CONCLUSIONS

It has been shown that the plasma crystal consisting of only two layers shows a transition from a solid state structure to a fluid or even gaslike state when the discharge conditions are changed, either by reducing the gas pressure or by raising the discharge power. The crystal is shown to be solid at a pressure of about 100 Pa and a power of 10–20 W. The melting of the crystal is demonstrated by the change in the positional and orientational correlation function. The correlations show a long-range order for the particle arrangement at pressures above 100 Pa and low power settings and decreasing order at reduced gas pressure or raised discharge power. Furthermore, the particles' motion during the transition is illustrated by the trajectory plots where stationary or streamline or irregular motion (only for pressure reduction) is observed. The melting is induced by the oscillatory and erratic motion of the particles in the lower layer. To this erratic motion a kinetic dust temperature can be assigned.

The measured values of the coupling parameter Γ with

the consideration of a measured dust kinetic temperature have been compared with the predictions of the Yukawa and the OCP model with satisfactory agreement. A comparison with theories of two-dimensional melting shows no strong evidence either for the hexatic phase of the KTHNY theory or for the first-order transition of the grain-boundary-induced melting.

ACKNOWLEDGMENTS

We like to thank V. A. Schweigert and I. V. Schweigert for helpful discussions and for material prior to publication. This work is supported by the DFG under Grant No. Pi185/8-1, which is gratefully acknowledged.

[1] G. S. Selwyn, J. Singh, and R. S. Bennett, J. Vac. Sci. Technol. A **7**, 2758 (1989).
[2] C. K. Goertz, Rev. Geophys. **27**, 271 (1989).
[3] E. Wigner, Trans. Faraday Soc. **34**, 678 (1938).
[4] H. Ikezi, Phys. Fluids **29**, 1764 (1986).
[5] J. H. Chu, J.-B. Du, and L. I, J. Phys. D **27**, 296 (1994).
[6] J. H. Chu and L. I, Physica A **205**, 183 (1994).
[7] J. H. Chu and L. I, Phys. Rev. Lett. **72**, 4009 (1994).
[8] H. Thomas, G. E. Morfill, V. Demmel, J. Goree, B. Feuerbacher, and D. Möhlmann, Phys. Rev. Lett. **73**, 652 (1994).
[9] A. Melzer, T. Trottenberg, and A. Piel, Phys. Lett. A **191**, 301 (1994).
[10] T. Trottenberg, A. Melzer, and A. Piel, Plasma Sources Sci. Technol. **4**, 450 (1995).
[11] C. A. Murray and D. H. V. Winkle, Phys. Rev. Lett. **58**, 1200 (1987).
[12] K. Strandburg, Rev. Mod. Phys. **60**, 161 (1988).
[13] S. G. Brush, H. L. Sahlin, and E. Teller, J. Chem. Phys. **45**, 2102 (1966).
[14] S. Ichimaru, Rev. Mod. Phys. **54**, 1017 (1982).
[15] M. O. Robbins, K. Kremer, and G. S. Grest, J. Chem. Phys. **88**, 3286 (1988).
[16] Produced by AERES GmbH, Rudower Chaussee 5, D-12484 Berlin, Germany.
[17] J. M. Kosterlitz and D. J. Thouless, J. Phys. C **6**, 1181 (1973).
[18] D. R. Nelson and B. I. Halperin, Phys. Rev. B **19**, 2457 (1979).
[19] A. P. Young, Phys. Rev. B **19**, 1855 (1979).
[20] S. T. Chui, Phys. Rev. B **28**, 178 (1983).
[21] D. Dubin, Phys. Rev. Lett.**71**, 2753 (1993).

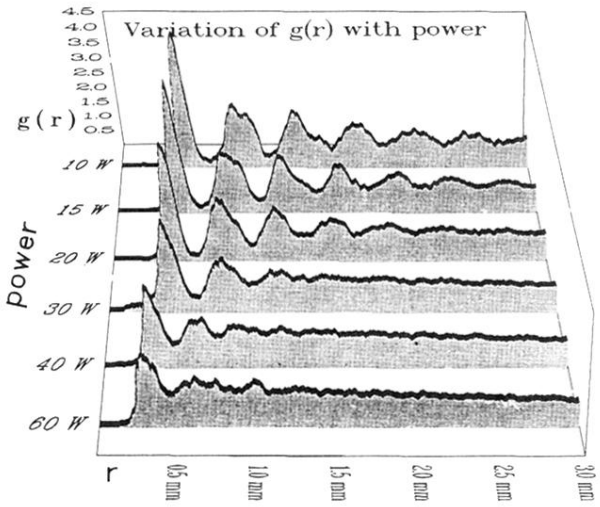

FIG. 11. Variation of the pair correlation function with power. The positional order decreases with power, but a gaslike state is not reached. Note that the nearest-neighbor distance is decreasing with power.

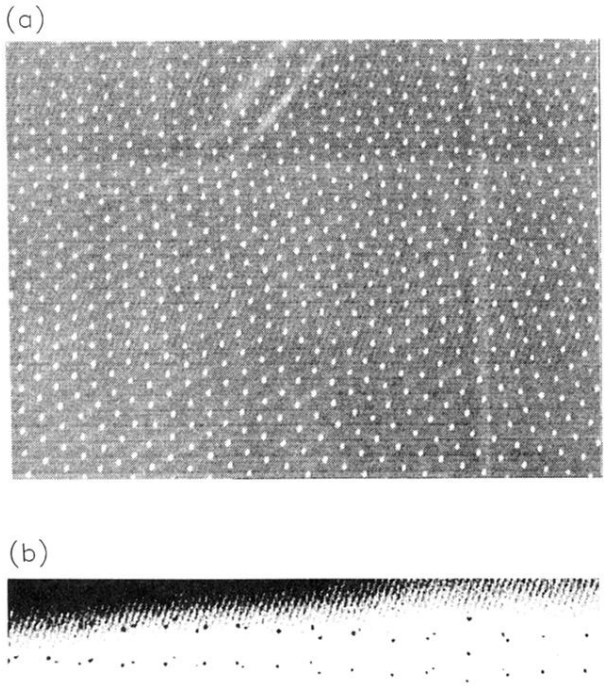

FIG. 2. Video images of the Wigner crystal at 118 Pa seen (a) from the top and (b) from the side (inverted image).

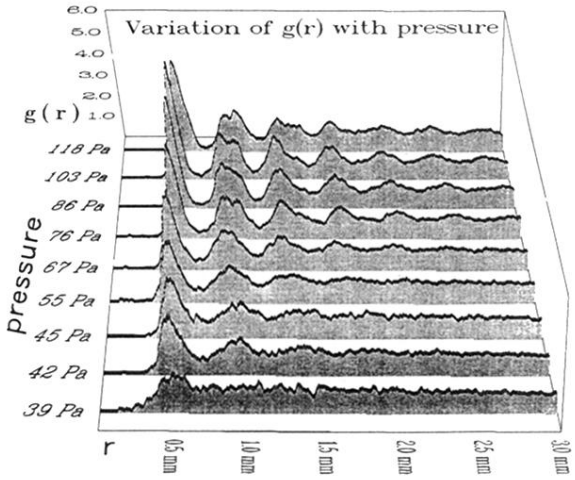

FIG. 4. Variation of the pair correlation function with pressure. At high pressure well ordered particles are observed. When decreasing the pressure the correlation becomes less. At 39 Pa the correlation function is almost that of an ideal gas.

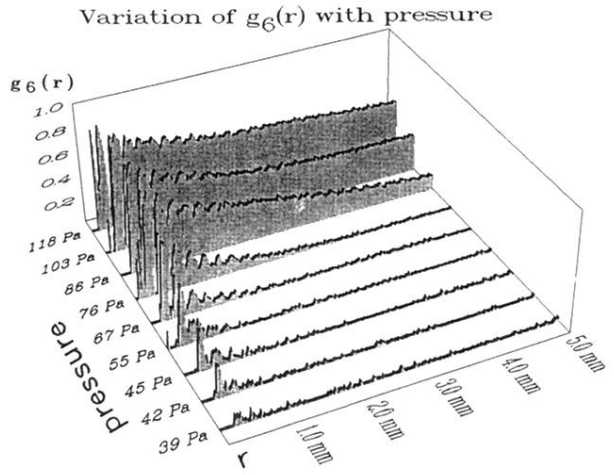

FIG. 9. Variation of the angular correlation function $g_6(r)$ with pressure. At higher pressure the correlation function is nearly constant and is rapidly decaying at lower pressure.